Journal of Materials Chemistry A

Accepted Manuscript

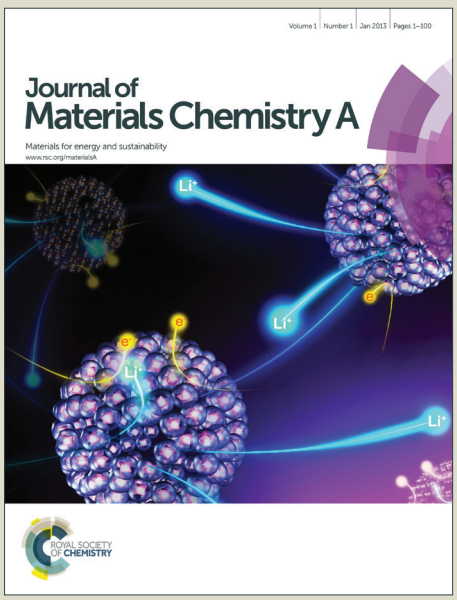

ROYAL SOCIETY OF CHEMISTRY

www.rsc.org/materialsA

Structural Tuning of Ancillary Chelate in Tri-carboxyterpyridine Ru(II) Sensitizers for Dye Sensitized Solar Cells

Chun-Cheng Chou,[a,‡] Pei-Hua Chen,[a,‡] Fa-Chun Hu,[a] Yun Chi,[a,*] Shu-Te Ho,[a] Ji-Jung Kai,[b,*] Shih-Hung Liu,[c] and Pi-Tai Chou[c,*]

[a] Department of Chemistry and Low Carbon Energy Research Center, National Tsing Hua University, Hsinchu 30013, Taiwan; E-mail: ychi@mx.nthu.edu.tw

[b] Department of Engineering and System Science, National Tsing Hua University, E-mail: jjkai@ess.nthu.edu.tw

[c] Department of Chemistry and Center for Emerging Material and Advanced Devices, National Taiwan University, Taipei 10617, Taiwan; E-mail: chop@ntu.edu.tw

[‡] C-C C and P-H C contributed equally to this work.

Abstract

Three distinctive classes of ancillary chelates, namely: 2-(3-trifluoromethylpyrazol-5-yl)-6-(4-trifluoromethylphenyl)pyridine (**L3**, H_2pzppy), 4-(pyrazol-5-yl)-2-(4-trifluoromethyl)phenylpyrimidine (**L5**, H_2pzppm) and 4-(6-(pyrazol-5-yl)pyridin-2-yl)-2-trifluoromethylpyrimidine (**L6**, H_2pzpypm), which showed identical skeletal topology, but with the more electronegative nitrogen atom replacing the isoelectronic methine group at the selected skeletal position, were obtained to investigate the photophysical and electrochemical properties and hence the associated Ru(II) sensitizers based DSC. To increase the optical absorptivity we also strategically added thiophene (thienyl) or 3,4-ethylenedioxythiophene (EDOT) appendages to **L6** for boosting short-circuit photocurrent (J_{SC}) and overall efficiency (η) of the fabricated DSC devices. Under AM 1.5G illumination the best sensitizer showed performance data of J_{SC} = 18.22 mA·cm^{-2}, V_{OC} = 0.66 V, FF = 0.729 and η =

8.72 %, and good cell stability at 60 °C for 1000 hours, being only decreased by ~5% in η value.

Introduction

The future prospect of a low-carbon society requires emerging renewable energy sources, among which the dye-sensitized solar cells (DSCs) are considered to be one competitive candidate. Especially, the low cost TiO_2 photoanode in DSCs can potentially be fabricated using printing technology, providing a viable alternative to conventional photovoltaics. Despite the development of a vast variety of different dyes to optimize the harvested solar photons, up to current stage, the Ru(II) based photosensitizers remain as the key component, because of the higher cell performance, particularly in view of stabilities versus other sensitizers such as organic donor-acceptor dyes and zinc porphyrin/phthalocyanine dyes.[1-5] Broadly speaking, the Ru(II) sensitizers constitute at least one *di*- or *tri*-carboxy substituted poly-pyridine chelate to serve as the anchor to the TiO_2 photoanode, plus an ancillary ligand which would modify both the light absorption capacity, ground state oxidation potential, and relative peak position of the metal-to-ligand charge transfer (MLCT) transition. Among a variety of Ru(II) based photosensitizers the thiocyanate-containing sensitizers N749 (or black dye),[6-8] Z907[9] and N719[10] represent three of the best known examples that have been tested for both fundamentals and commercial applications.

From the viewpoint of device stability, the robust skeletal framework of sensitizers is considered as a major factor governing the lifespan. Thus, studies on the thiocyanate-free Ru(II) sensitizers with either dicarboxy bipyridine or tricarboxy terpyridine anchor are emerged in recent years.[11-22] The thiocyanate is expected to undergo dissociation from sensitizer in solution due to its latent activity against ligand exchange.[23] To mitigate this problem, a new class of Ru(II) sensitizers were synthesized with the thiocyanates replaced by either electron-deficient cyclometalate[24-27] or chelating azolate.[28-30] This approach is stimulated by the general

believes that the chelates should be less labile compared to the uni-dentate bonding of thiocyanate, and the fact that the added electron deficiency is capable to increase the ground state oxidation potential of sensitizers for faster dye regeneration by I^-/I_3^- redox couple.

Recently, our interests have extended to the *bis*-tridentate Ru(II) sensitizer.[31-35] We started with a series of multidentate ancillary chelates, namely: 2,6-bis(3-trifluoromethylpyrazol-5-yl)pyridine (**L1**, H_2pz_2py), 2,6-bis(3-trifluoromethyl-1,2,4-triazol-5-yl)pyridine (**L2**, H_2tz_2py), 2-(3-trifluoromethylpyrazol-5-yl)-6-(4-trifluoromethylphenyl)pyridine (**L3**, H_2pzppy) and 2-(3-trifluoromethyl-1,2,4-triazol-5-yl)-6-(4-trifluoromethylphenyl)pyridine (**L4**, H_2tzppy), which are synthesized and employed in construction of relevant Ru(II) sensitizers (see Scheme 1). Their outstanding DSC performances were subsequently validated by showing optimal light harvesting capability down to the near-IR region. Motivated by this finding, we then launched a study on synthesizing new multidentate ancillaries to further fine-tune their electrochemical and spectroscopic properties by insertion of nitrogen atom at specific positions of the backbone, and to explore the associated cell performances.

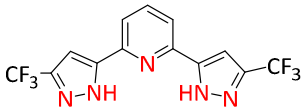

L1: H_2pz_2py

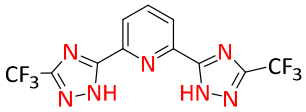

L2: H_2tz_2py

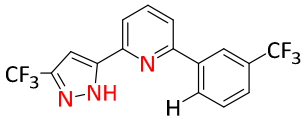

L3: H_2pzppy

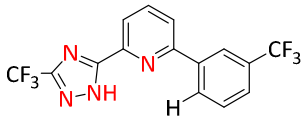

L4: H_2tzppy

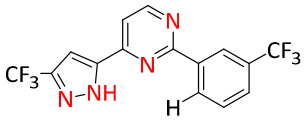

L5: H_2pzppm

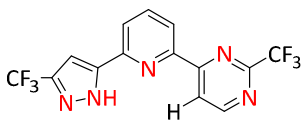

L6: $H_2pzpypm$

Scheme 1. Structures of the ancillary chelates in various *bis*-tridentate Ru(II) sensitizers.

In this paper, we present two new classes of ancillary chelates, namely: 4-(pyrazol-5-yl)-2-(4-trifluoromethyl)phenylpyrimidine (**L5**, H_2pzppm) and 4-(6-(pyrazol-5-yl)pyridin-2-yl)-2-trifluoromethylpyrimidine (**L6**, H_2pzpypm). Their structures differ by incorporation of one pyrimidine fragment as opposed to the central pyridine fragment or at the terminal phenyl group in the parent **L3** ancillary (Scheme 1). We then probe this subtle structural change versus the critical effect on the DSC performance. Moreover, substituted thiophene (thienyl) or 3,4-ethylenedioxythiophene (EDOT) appendages were also added to the **L6** ancillary in an aim to increase optical absorptivity and hence boost short-circuit photocurrent (J_{SC}) and overall efficiency (η) under AM 1.5G illumination.

Results and discussion

First, the demanded dianionic tridentate ancillaries were prepared via the multi-step protocols depicted in Schemes 2 ad 3. For the H_2pzppm chelate **L5**, the first step is to replace the 4-chloro substituent of 2,4-dichloropyrimidine with a methoxide protecting group by a simple nucleophilic substitution,[36] followed by replacement of the unprotected 2-chloro substituent with the *m*-trifluoromethylphenyl group using Suzuki cross-coupling reaction.[37] The subsequent conversion of 4-methoxy group back to the chloro substituent is achieved using chlorination reagent $POCl_3$.[38] The resulting chloride compound was subjected to cyanation using KCN,[39] followed by methylation with Grignard reagent to afford the acetyl group.[40] Finally, this acetyl group was converted to the pyrazole moiety using Claisen condensation and hydrazine cyclization in sequence.[41]

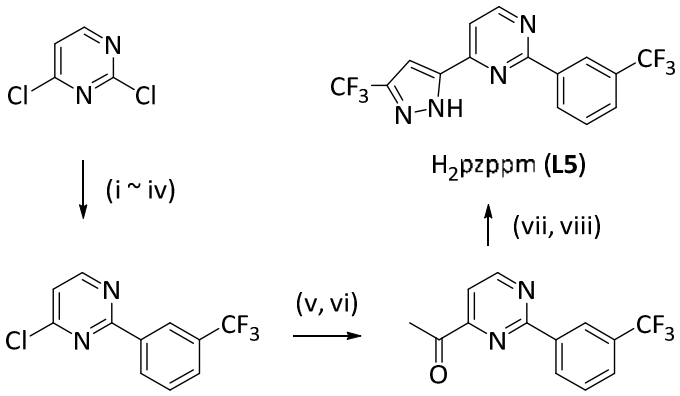

Scheme 2. Synthetic protocols: (i) NaOMe, MeOH; (ii) 3-(trifluoromethyl)phenyl boronic acid, $[Pd(PPh_3)_4]$, Na_2CO_3, THF-H_2O; (iii) $HCl_{(aq)}$; (iv) $POCl_3$, toluene; (v) KCN, DABCO, DMSO-H_2O; (vi) CH_3MgBr, THF, $HCl_{(aq)}$; (vii) NaOEt, CF_3CO_2Et, THF; (viii) N_2H_4, EtOH.

On the other hand, the H_2pzpypm chelate **L6** and its thienyl and EDOT functionalized derivatives, i.e. **L6.1**: R = 5-hexyl-2-thienyl and **L6.2**: R = 7-hexyl-2,3-dihydrothieno[3,4-*b*]-1,4-dioxin-5-yl, were prepared using another synthetic sequences starting from 2,6-diacetylpyridine and derivatives, see Scheme 3. One acetyl substituent was first protected using stoichiometric amount of ethylene glycol in presence of acid catalyst;[42] the second (unprotected) acetyl group was sequentially reacted with N,N-dimethylformamide dimethyl acetal, trifluoroacetamidine and sodium ethoxide to induce the formation of a CF_3-substituted pyrimidine fragment.[43] After then, the dioxolane group was hydrolyzed to release the acetyl group.[44] It was then reacted with ethyl trifluoroacetate under condition for Claisen condensation, followed by hydrazine cyclization to afford the anticipated pyrazole group.[41]

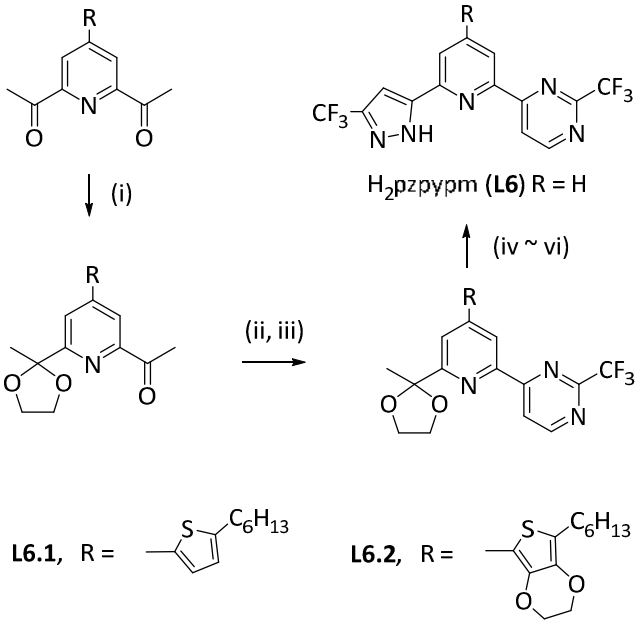

Scheme 3. Synthetic protocols: (i) ethylene glycol; (ii) N,N-dimethylformamide dimethyl acetal; (iii) trifluoroacetamidine, NaOEt, EtOH; (iv) $HCl_{(aq)}$; (v) NaOEt, CF_3CO_2Et, THF; (vi) N_2H_4, EtOH.

With these ancillary chelates in hands, the demanded *bis*-tridentate Ru(II) sensitizers can be synthesized from coupling of $Ru(tectpy)Cl_3$ (tectpy = 4,4',4"-triethoxycarboxy-2,2':6',2"-terpyridine) and ancillary chelate in presence of KOAc. Specifically, the designated Ru(II) sensitizers **TF-25**, **26**, **27** and **28** are synthesized using the aforementioned chelates **L5**, **L6**, **L6.1** and **L6.2**, respectively. Their molecular structures, together with that of reference sensitizer **TF-21**, are depicted in Scheme 4.

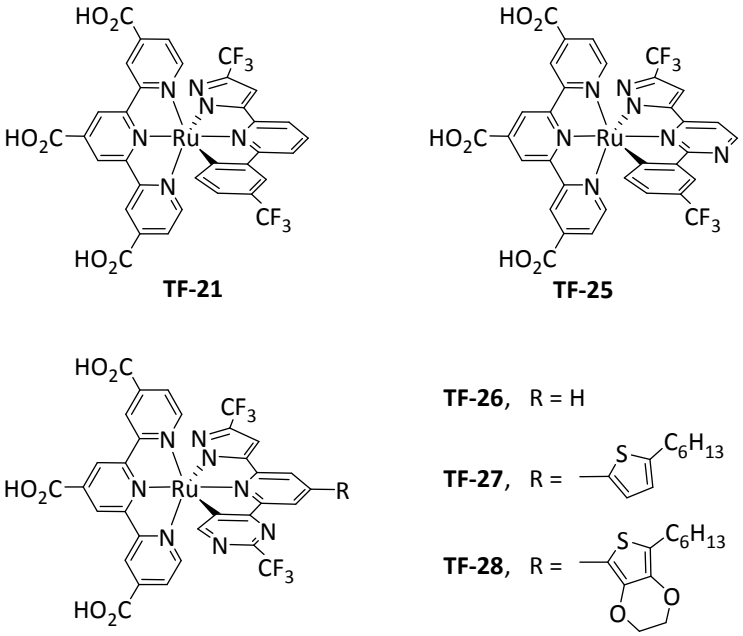

Scheme 4. Structures of Ru(II) sensitizers **TF-25** ~ **TF-28** and **TF-21** reference.

The UV-Vis absorption spectra of sensitizers **TF-25** ~ **TF-28** in DMF (dimethylformamide) at conc. of 1×10^{-5} M are depicted in Figure 1, together with the spectrum of **TF-21** as the reference, while the photophysical and cyclic voltammetric data are listed in Table 1. Generally speaking, **TF-21** exhibited two sharp MLCT bands at 404 nm and 521 nm, together with a longer wavelength shoulder that showed a slow decrease in intensity and extended all the way to the near infrared (> 800 nm). In accordance with this pattern, both **TF-25** and **TF-26** depicted two MLCT absorptions at ~400 and ~520 nm, with extinction coefficient of the lower energy MLCT band (1.2×10^4 L·mol^{-1}cm^{-1}) being slightly lower than that of the higher energy one (1.5×10^4 L·mol^{-1}cm^{-1}), and a much faster decline in intensity for the lower energy MLCT shoulder versus that of **TF-21**. Furthermore, upon addition of thienyl and EDOT group to **TF-26**, the resulting sensitizers **TF-27** and **TF-28** give the lower energy MLCT peak maxima at around 530 and 533 nm, i.e. with a bathochromic shift of at least 13 nm versus that of **TF-26**, and a substantial gain in absorptivity to ε = 2.1 ~ 2.3 $\times$ 10^4 L·mol^{-1}cm^{-1}. This could imply a better light

harvesting capability for **TF-27** and **TF-28** over that of the parent **TF-26**, which is consistent with the influence of the attached electron donating and π-conjugating appendage observed in many organic push-pull and Ru(II) based sensitizers.[45-52]

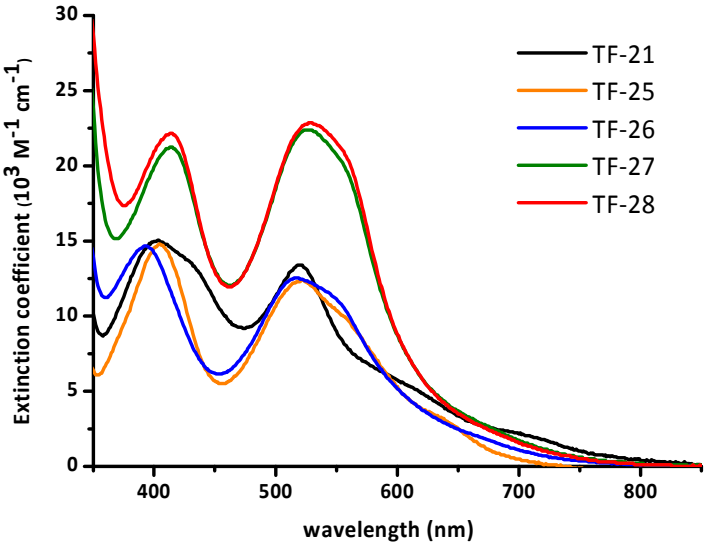

Figure 1. UV-Vis absorption spectra of Ru(II) sensitizers **TF-25** ~ **TF-28** and reference **TF-21** at 1×10^{-5} M in DMF at RT.

Calculations based on density functional theory (DFT) and time-dependent DFT in DMF were performed for the titled complexes. Figures 2 and 3 depict the simulation of the absorption wavelengths (vertical line) and the relative transition probability (magnitude of vertical line) of **TF-25** ~ **TF-28** (please see the result of **TF-21** in reference [33]). Also depicted in these Figures are the frontier orbitals contributed to the major electronic transition recorded. All numerical data for vertical transition and comprehensive frontier orbital analyses are listed in Tables S1 – S4 and Figures S1 – S4 of Supporting Information. As a result, the peak wavelength over 500 nm is calculated to be 529, 521, 522, and 525 nm for **TF-25** ~ **TF-28**, respectively, for which both value and trend are consistent with the experimental absorption maximum for **TF-25** (523 nm), **TF-26** (517 nm), **TF-27** (530 nm) and **TF-28** (533 nm) in DMF (see Table 1), supporting the validity of computational approaches. Careful examination of the optical transition and its associated frontier orbitals

indicates that the lower lying singlet transitions over 500 nm are mainly contributed by metal-to-ligand (tricarboxy-terpyridine) charge transfer (MLCT), together with a minor part of ancillary to anchor (terpyridine) charge transfer (LLCT). In the higher lying transition around 400 ~ 550 nm, the unoccupied orbitals of thienyl (**TF-27**) and EDOT (**TF-28**) appendages have imposed appreciable contribution (see Figure 3) due to an elongation of π-conjugation, [53-56] which rationalizes the substantial gain of absorptivity as well as the red shift of peak wavelength observed experimentally for **TF-27** and **TF-28** in this region.

Table 1. Photophysical and electrochemical data for the studied Ru(II) sensitizers.

dye	λ_{abs} [nm] (ε [10^3 L·mol^{-1}cm^{-1}]) [a]	$E_{ox}°'$ (V) [b]	$E_{0\text{-}0}$ (eV)	$E°'*$ (V)
TF-21	404 (15), 520 (13), 703 (2.2)	0.84	1.62	-0.78
TF-25	405 (15), 523 (12), 555 (10)	0.93	1.72	-0.79
TF-26	393 (15), 517 (12), 548 (11)	0.96	1.75	-0.79
TF-27	415 (21), 530 (22), 558 (20)	0.96	1.72	-0.76
TF-28	415 (22), 533 (23), 558 (21)	0.94	1.74	-0.80

[a] Absorption and emission spectra were measured at 1×10^{-5} M in DMF. [b] Oxidation potential of dyes was measured in DMF with 0.1 M [TBA][PF_6] and a scan rate of 50 mV s^{-1}. It was calibrated with Fc/Fc$^+$ as internal standard and converted to NHE by addition of 0.63 V.

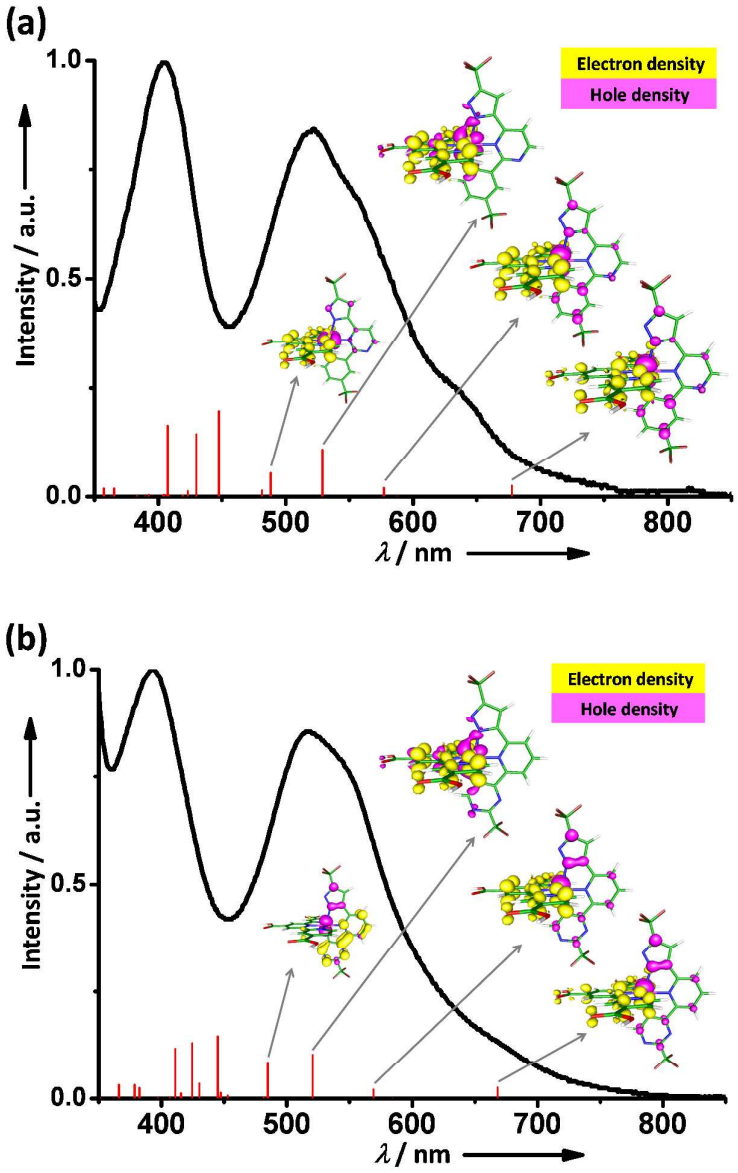

Figure 2. The absorption spectra of (a) **TF-25** and (b) **TF-26** sensitizers. Also depicted are the TD-DFT calculated absorption wavelengths (vertical line) and the relative transition probability (magnitude of vertical line). Inset: the selected frontier orbitals contributed to the major transitions. The occupied and unoccupied orbitals are represented in pink and yellow, respectively.

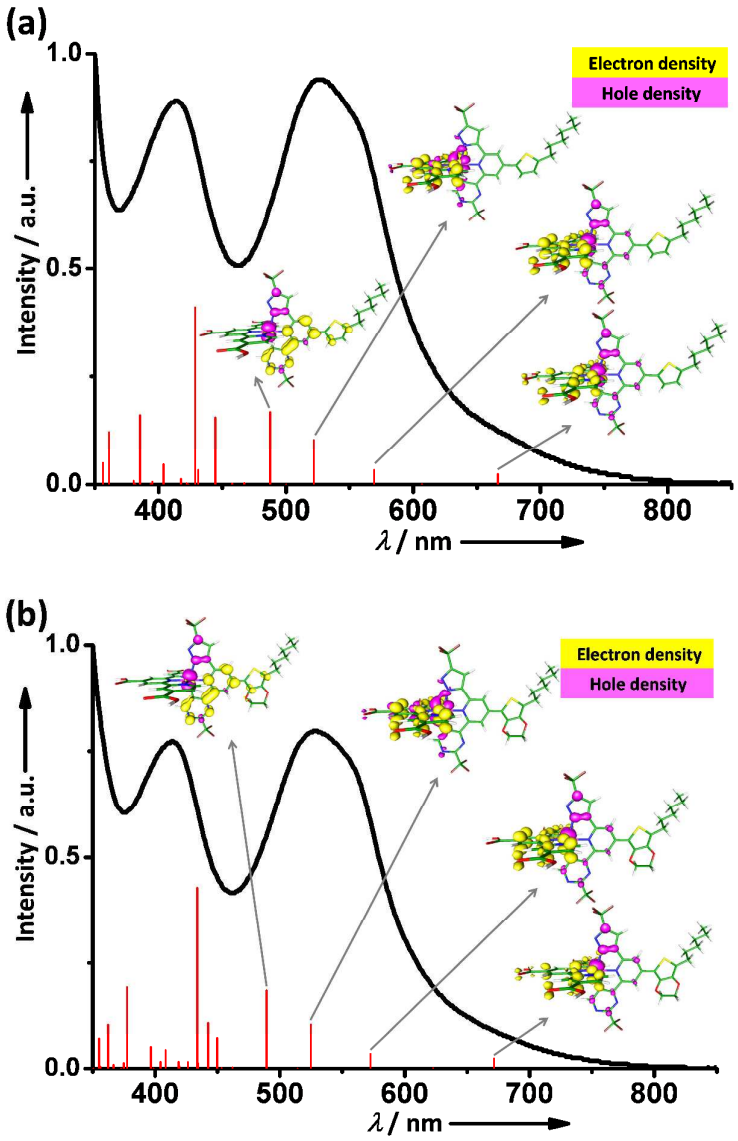

Figure 3. The absorption spectra of (a) **TF-27** and (b) **TF-28** sensitizers. Also depicted are the TD-DFT calculated absorption wavelengths (vertical line) and the relative transition probability (magnitude of vertical line). Inset: the selected frontier orbitals contributed to the major transitions. The occupied and unoccupied orbitals are represented in pink and yellow, respectively.

Cyclic voltammetry was conducted to reveal their ground state oxidation potential ($E_{ox}^{\circ\prime}$). With the $E_{ox}^{\circ\prime}$ data in hand, the corresponding excited state oxidation potentials ($E^{\circ\prime}$*) were estimated using the equation $E^{\circ\prime}* = E_{ox}^{\circ\prime} - E_{0\text{-}0}$, for

which $E_{0\text{-}0}$ stands for the optical energy gap, i.e. at 5% onset of their lowest energy absorption. In general, the absorption onset of **TF-25** and **TF-26** show a significant hypsochromic shift than that of **TF-21**, resulting in the higher onset energy by 0.1 eV. However, this increase in $E_{0\text{-}0}$ was offset by the more positive E_{ox}°′ of **TF-25** and **TF-26** recorded (0.93 and 0.96 V), leaving the respective $E^{\circ\prime}$* essentially unchanged. Moreover, the **TF-27** and **TF-28** sensitizers are modified by addition of thienyl and EDOT appendage to **TF-26**. Although this functionalization red shifts the higher lying MLCT/ππ* absorptions as well as simultaneously increases the extinction coefficient, their $E_{ox}^{\circ\prime}$ values are virtually unaltered versus that of **TF-26** (see Table 1). Moreover, as shown in Figure 1, the onset of the absorption, i.e., $E_{0\text{-}0}$, is nearly the same among **TF-26**, **TF-27** and **TF-28**. Support of this also provided by computational results, in which the calculated $S_0 \rightarrow S_1$ transition is virtually identical, being 668, 666 and 671 nm for **TF-26**, **TF-27** and **TF-28**, respectively (see Tables S2 ~ S4). The result also reconfirms the aforementioned viewpoint that the added thienyl (**TF-27**) and EDOT (**TF-28**) appendages only affect the higher lying excited state, while the lowest lying excited state is only dominated by Ru(II)-to-anchor (tricarboxy-terpyridine) MLCT transition. The invariance of E_{ox}°′ and $E_{0\text{-}0}$ leads to similar $E^{\circ\prime}$* for **TF-26** ~ **28**. For all these newly developed Ru(II) complexes, evidently, the obtained $E_{ox}^{\circ\prime}$ and $E^{\circ\prime}$* are sufficiently more positive and negative than that of the redox potential of I^-/I_3^- couple (ca. 0.35 V vs. NHE) as well as the corresponding conduction band edge of the TiO_2 electrode (ca. −0.7 V vs. NHE) [27, 57] respectively, confirming their suitability to serve as the suitable DSC sensitizers.

DSCs were next fabricated using these sensitizers absorbed on the TiO_2 photoanode that consists of a 15 μm layer of 20 nm absorbing particles and 7 μm layer of 400 nm light scattering particles, deposited with multiple screen-printing manipulation.[33] Moreover, the sensitizers were dissolved in mixed EtOH and DMSO (*v/v* 4:1) to afford a 0.3 mM solution, together with the addition of 1 mM chenodeoxycholic acid (CDCA) as coadsorbent to reduce the dye aggregation. The

electrolyte solution, coded A, consists of 2.0 M 1,3-dimethylimidazolium iodide (DMII), 0.1 M guanidinium thiocyanate (GuNCS), 0.05 M LiI, 0.03 M I_2, and 0.5 M 4-*tert*-butylpyridine (tBP) in acetonitrile and valeronitrile (*v/v*, 85:15). Prior to the measurement, the solar simulator (Sun 3000, ABET Technologies) was calibrated with a certificated *c*-Si solar cell equipped with a KG-3 filter.[58] Device performances were measured using a metallic shadow mask with a square aperture of 4 × 4 mm^2. The obtained photovoltaic parameters are listed in Table 2. It is notable that the recorded cell efficiency of **TF-21** is similar to the previously reported data,[33] while obviously all the newly developed complexes **TF-25** ~ **TF-28** have shown improved efficiencies. This appears to be due to the more positive $E_{ox}^{\circ\prime}$, i.e., higher oxidation potential versus **TF-21**, so that faster dye regeneration is expectable, giving better cell efficiency.[59-61]

Table 2. The performance characteristics of DSCs using electrolyte A and under AM 1.5G illumination.

Sensitizers	J_{SC} [$mA \cdot cm^{-2}$]	V_{OC} [V]	FF	η [%]	dye loading[a] [$\times 10^{-7}$ $mol \cdot cm^{-2}$]
TF-21	10.54	0.58	0.704	4.31	1.42 ± 0.08
TF-25	15.25	0.64	0.709	6.92	1.55 ± 0.08
TF-26	15.34	0.63	0.733	7.08	1.42 ± 0.06
TF-27	12.04	0.59	0.748	5.32	0.88 ± 0.01
TF-28	13.19	0.61	0.746	6.00	0.79 ± 0.01

[a] The value is calculated from the MLCT band ratio for desorbed dye solution versus (0.01 mM) reference solution in mixed MeOH and water (*v/v*, 1:1) added with 0.1 M of TBAOH.

The device was further improved by adding tetrabutylammonium deoxycholate [TBA][DOC] to the dye solution, and switching to a different electrolyte system. The addition of co-adsorbent [TBA][DOC] is expected to conduct the proton-to-TBA exchange at the sensitizer, which in turn could improve the solubility and shift the $E^{\circ\prime}$* to a more negative value.[62, 63] In this approach the alternative

electrolyte, now is coded B, consists of 0.6 M 1,2-dimethyl-3-propylimidazolium iodide (DMPII), 0.1 M LiI, 0.05 M I_2, and 0.5 M 4-*tert*-butylpyridine (tBP) in acetonitrile and valeronitrile (*v/v*, 85:15). The higher concentration of LiI in electrolyte B is expected to lower the conduction band edge of TiO_2 and lead to faster electron injection and higher J_{SC} for the DSC devices. [64-67]

The resulting photovoltaic parameters are listed in Table 3. For confirming the increase of both solubility and dye loading by the addition of [TBA][DOC], we re-measured the dye loading under this new condition. As expected, the loading of **TF-21** is notably increased by 19% and this reference **TF-21** device now affords better improved conversion efficiency (η) of 6.44%. In the meantime, DSCs of respective **TF-25** and **TF-26** under the same condition also demonstrate higher loading and much improved efficiencies; namely: η of 7.86 and 7.85%, J_{SC} of 16.92 and 17.12 mA·cm^{-2}, V_{OC} of 0.68 and 0.63 V, and fill factor (FF) of 0.683 and 0.728, as shown in Table 3. The superiority in **TF-25** and **TF-26** over that of **TF-21** is also attributed to the electron withdrawing property of extra nitrogen atoms in the ancillary that shifted the $E_{ox}°'$ to the more positive value for faster dye regeneration (Table 1).[59-61] Moreover, since both **TF-25** and **TF-26** show nearly identical efficiency, the result implicates that the location of the pyrimidinyl substituent imposes insignificant variation in device efficiency due to the retention of both spatial and electrochemical properties.

Upon further modification of **TF-26** by decoration of either thienyl (**TF-27**) or EDOT (**TF-28**) substituent, the device efficiency increases to 7.92% for **TF-27** and more prominently to 8.72% for **TF-28**. This improvement is attributed to both better dye loading and light harvesting effect, but the increment is smaller for the thienyl derivative **TF-27** than that of the EDOT functionalized **TF-28**. While the exact cause is unclear, we suspect it could be related to the faster charge recombination,[68] which reduced both J_{SC} and V_{OC}, as shown by the inferior device performance of **TF-27** (η = 5.32 %) vs. that of **TF-26** (η = 7.08 %) and **TF-28** (η = 6.00 %) recorded under lower

dye loading and with electrolyte A (cf. Table 2).

Table 3. The performance characteristics of DSCs using electrolyte B and under AM 1.5G illumination.

Sensitizers	J_{SC} [mA·cm^{-2}]	V_{OC} [V]	FF	η [%]	dye loading [$\times 10^{-7}$ mol·cm^{-2}]
TF-21	15.41	0.64	0.654	6.44	1.69 ± 0.08
TF-25	16.92	0.68	0.683	7.86	2.11 ± 0.05
TF-26	17.12	0.63	0.728	7.85	1.89 ± 0.07
TF-27	17.43	0.62	0.733	7.92	1.04 ± 0.05
TF-28	18.11	0.66	0.729	8.72	1.05 ± 0.04
N749	16.92	0.72	0.727	8.86	

The corresponding J-V characteristics and IPCE action spectra are shown in Figure 4. The IPCE profile of all sensitizers (i.e. **TF-25** ~ **TF-28**) clearly reveals significant improvement over that of **TF-21** in the region 400 – 700 nm, and we attribute this to the more positive E_{ox}°' and the higher driving force for dye regeneration with iodide-electrolyte. In Figure 3(b), the **TF-28** sensitizer with an EDOT appendage showed the highest J_{SC} of 18.11 mA cm^{-2}, which is also in agreement with the higher IPCE (by an deviation of < 10%) over the solar spectral region. Thus, coupled with V_{OC} of 0.66 V and FF of 0.729, **TF-28** gave the highest conversion efficiency of 8.72%. On the other hand, **TF-27** device did not perform equivalent efficiency despite of showing similar spectrum profile and absorptivity versus that of **TF-28**.

For showing intimate comparison to pristine sensitizer **N749**, we also fabricated a reference DSC device using identical cell parameters and electrolyte B (cf. Table 3). This reference device showed an essentially identical value of overall efficiency, but with a slightly lower J_{SC} and higher V_{OC} versus our best sensitizer **TF-28** in this study. The variations of J_{SC} and V_{OC} between **TF-28** to **N749** could be due to the better light harvesting property and faster charge recombination, a result of the introduction of

EDOT appendage at the ancillary chelate of **TF-28**.

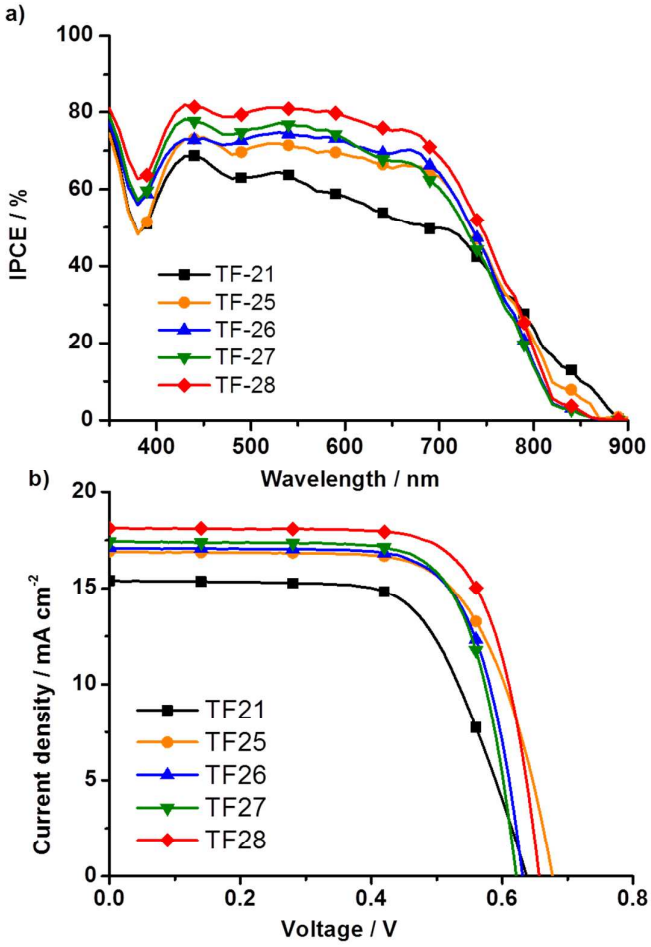

Figure 4. IPCE action diagram and *J-V* characteristics for devices fabricated using the electrolyte B.

To further probe the device performances, measurements of charge extraction (CE) and transient photovoltage (TPV) decay were carried out, for which relevant data are shown in Figure 5(a) and (b). Differences in V_{OC} between cells can generally be explained by shifts in the TiO_2 conduction band edge (manifested by the shift of the exponential distribution of experimental data measured by CE) and/or by TiO_2 recombination lifetimes (investigated via TPV measurements).[69, 70] As can be seen, except for **TF-21** which has a slightly lower V_{OC} at a fixed photo-induced charge

density due to a downward shift of the band edge, all other DSC devices show very similar V_{OC}, indicating that the conduction band potentials are similar in cells **TF-25** ~ **TF-28**. In Figure 5(b), transient photovoltage measurements at a fixed charge density indicate that device made by **TF-25** has the longest electron lifetime, while **TF-27** is the shortest among all others. The trend of electron lifetime of these TF sensitizers seems to be in good agreement with the V_{OC} of the devices (Table 2), suggesting that the conduction band edge of TiO_2 is less influential to the observed V_{OC}.

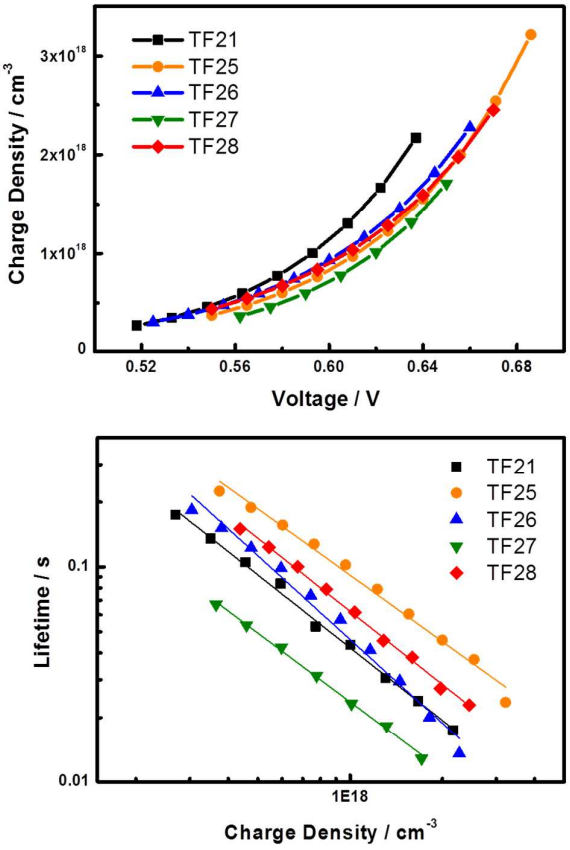

Figure 4. (a) TiO_2 electron density versus voltage deduced from charge extraction measurements and (b) electron lifetime versus TiO_2 electron density deduced from transient photovoltage measurements for DSC devices containing **TF-21** and **TF-25** ~ **TF-28** dyes. The cell voltage is controlled via tuning the illumination from a halogen lamp.

Then, electrochemical impedance spectroscopy was also utilized to analyze the resistance to charge recombination in these devices. Figure 5 shows the Nyquist plots measured in dark at a forward bias same as the respective V_{OC} tested under one-sun illumination. The impedance spectra are composed of 2 semicircles, in which the left (smaller cycle) one depicts the electrochemical reaction at the Pt/electrolyte interface, and the right (larger cycle) one represent the impedance characteristics of the charge recombination (R_r) at the TiO_2/dye/electrolyte interface.[71-73] The radii of the right series of semicircles indicates R_r to be in the order of **TF-25** > **TF-28** > **TF-21** > **TF-26** ≈ **TF-27** and, thus, the dark currents (J_{dark}) appear an inverse trend, which are consistent with the previous TPV results.

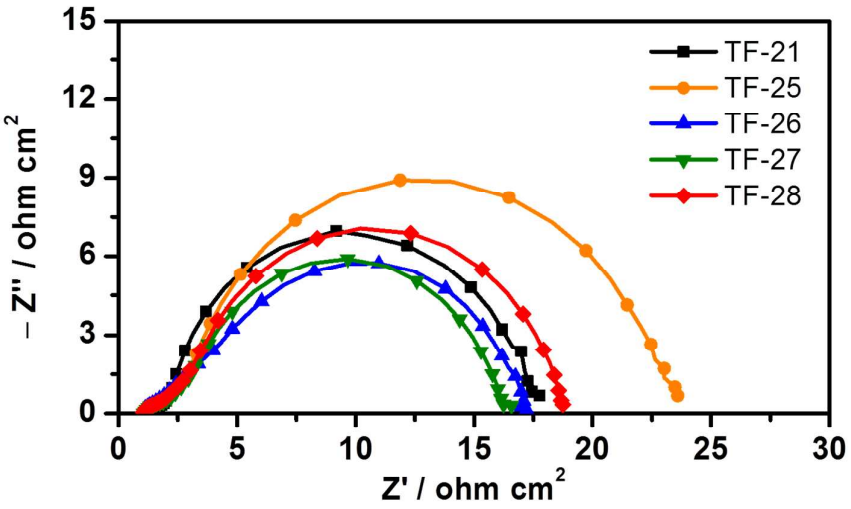

Figure 5. Electrochemical impedance spectra of DSC devices tested in dark with an external bias as each corresponding V_{OC} under one-sun illumination.

To test the stability of Ru(II) sensitizers, the highest efficiency **TF-28** device was subjected to light soaking test at 60 °C for 1000 h after adopting a low-volatility electrolyte consisting of the composition of 0.6 M PMII, 0.15 M I_2, 0.1 M GuNCS, and 0.5 M NBB (N-butyl-1*H*-benzimidazole) in butyronitrile (BN).[74] In a duration of 1000 h, the J_{SC}, V_{OC}, FF, and η were steady until 600 h and then decreased. The η_{max} of 7.87%

located around 500 h. The decline of efficiency, defined as $(\eta_{max} - \eta_{1000h})/\eta_{max}$, is 5.2% which is closed to other data reported by our group.[33] This result reconfirms that *bis*-tridentate architecture is stable against the applied thermal stress under simulated solar irradiation.

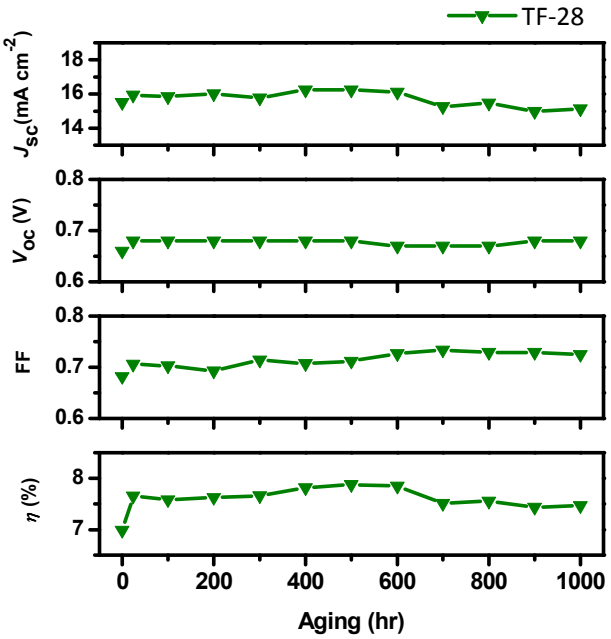

Figure 6. Device performances of **TF-28** under one-sun light soaking at 60 °C for 1000 h.

Conclusion

In summary, two new types of terdentate ancillary ligands, namely: H_2pzppm (**L5**) and H_2pzpypm (**L6**) and derivatives (**L6.1** and **L6.2**), were synthesized and employed to construct four *bis*-tridentate, thiocyanate-free Ru(II) complexes **TF-25** ~ **TF-28**. The substitution of pyrimidine for pyridinyl and phenyl group in reference **TF-21,** yielding **TF-25** and **TF-26**, respectively, has successfully increased the ground state oxidation potentials to a level of 0.93 – 0.96 V (vs. NHE). With addition of thienyl and EDOT decorations on H_2pzpypm ancillary, the resulting **TF-27** and **TF-28** sensitizers exhibit the expected hyperchromic and bathochromic effects, respectively, on their UV-Vis

absorption spectra. The devices made by **TF-25** ~ **28** all have superior performance over that of **TF-21**. **TF-27** showed an improved efficiency up to 7.92%, while **TF-28** demonstrates the highest efficiency of 8.72%, with an average IPCE of 80% over 400 – 700 nm and an onset wavelength of 860 nm, confirming their usefulness as guideline for fine-tuning the functional DSC sensitizers.

Experimental section

General Procedures. All reactions were performed under nitrogen. Solvents were distilled from appropriate drying agents prior to use. Commercially available reagents were used without further purification. All reactions were monitored by TLC with pre-coated silica gel plates (Merck, 0.20 mm with fluorescent indicator UV254). Compounds were visualized with UV irradiation at 254 or 365 nm. Flash column chromatography was carried out using silica gel obtained from Merck (230 - 400 mesh). Mass spectra were obtained on a JEOL SX-102A instrument operating in electron impact (EI) or fast atom bombardment (FAB) mode. ^{1}H and ^{19}F NMR spectra were recorded on a Bruker-400 or INOVA-500 instrument; chemical shifts are quoted with respect to the internal standard tetramethylsilane. Elemental analysis was carried out with a Heraeus CHN-O Rapid Elementary Analyzer. Photophysical data were obtained using an Edinburgh Fluorescence spectrometer FLS928P. Details of the synthetic protocols for the tri-dentate ancillary chelates and the procedures for the DSC cell fabrication and measurement are all given in the electronic supporting information.

Synthesis of TF-25. A mixture of 4-(3-(trifluoromethyl)-1H-pyrazol-5-yl)-2-(3-(trifluoromethyl)phenyl) pyrimidine (114 mg, 0.32 mmol), Ru(tectpy)Cl_3 (204 mg, 0.32 mmol) and KOAc (156 mg, 1.60 mmol) in 30 mL of xylenes was heated at 140°C under stirring for 15 h. After the removal of solvent, the crude product of TF-25-Et was purified by silica gel column chromatography (ethyl acetate/hexane = 1:2). After

then, the resulting solid was dissolved in a mixture of acetone (20 mL) and 1N NaOH solution (1.0 mL). For hydrolysis, the mixture was stirred at room temperature under nitrogen for 5 h. The solvent was removed, and the residue was dissolved in H_2O solution (5 mL). This solution was titrated with 2N $HCl_{(aq)}$ to pH = 3 to afford a brown precipitate. This brown product was washed with acetone and ethyl acetate in sequence, to yield, giving the final product. Yield: 187 mg, 72%. All other Ru(II) derivatives, e.g. **TF-26** ~ **TF-28**, were synthesized from Ru(tectpy)Cl_3 and respective ancillary chelates using identical procedures.

Selected spectral data of **TF-25**. MS (FAB, ^{102}Ru): m/z 824 (823) $[M+1]^+$. ^{1}H NMR (400 MHz, d_6-DMSO,298 K): δ 9.39 (s, 2H), 9.15 (s, 2H), 8.14 ~ 8.16 (m, 2H), 7.60 ~ 7.63 (m, 4H), 7.47 (s, 1H), 6.76 (d, J_{HH} = 7.6 Hz, 1H), 5.68 (d, J_{HH} = 8 Hz, 1H); ^{19}F NMR (376 MHz, d_6-DMSO, 298 K): δ -58.54 (s, 3F), -60.64 (s, 3F). Anal. Calcd. for $C_{33}H_{17}F_6N_7O_6Ru{\cdot}2H_2O$: C, 46.16; N, 11.42; H, 2.47. Found: C, 46.09; N, 11.31; H, 2.15.

Selected spectral data of **TF-26**. MS (FAB, ^{102}Ru): m/z 825 $(M+1)^+$. ^{1}H NMR (400 MHz, d_6-DMSO, 298 K): δ 9.31 (s, 2H), 9.11 (s, 2H), 8.33 ~ 8.28 (m, 2H), 8.22 (t, J_{HH} = 8 Hz, 1H), 7.64 (dd, J_{HH} = 6 Hz, 2H), 7.59 (d, J_{HH} = 6 Hz, 2H), 7.26 (s, 1H), 7.13 (s, 1H). ^{19}F NMR (376 MHz, d_6-DMSO, 298 K): δ -58.36 (s, 3F), -68.33 (s, 3F). Anal. Calcd. for $C_{32}H_{16}F_6N_8O_6Ru{\cdot}2H_2O$: C, 44.71; N, 13.04; H, 2.35. Found: C, 44.79; N, 12.70; H, 2.46.

Selected spectral data of **TF-27**. MS (FAB, ^{102}Ru): m/z 991 $(M+1)^+$. ^{1}H NMR (400 MHz, d_6-DMSO, 298 K): δ 9.32(s, 2H), 9.12(s, 2H), 8.64 (s, 1H), 8.27 (s, 1H), 8.02 (d, J_{HH} = 3.6 Hz, 1H), 7.70 (d, J_{HH} = 6 Hz, 2H), 7.63 (d, J_{HH} = 6 Hz, 2H), 7.41 (s, 1H), 7.15 (s, 1H), 7.11 (d, J_{HH} = 3.6 Hz, 1H), 2.95 (t, J_{HH} = 8 Hz, 2H), 1.74 (quin, J_{HH} = 8 Hz, 2H), 1.40 ~ 1.31 (m, 6H), 0.89 (t, J_{HH} = 8 Hz, 3H). ^{19}F NMR (376 MHz, d_6-DMSO, 298 K): δ -58.38 (s, 3F), -68.22 (s, 3F). Anal. Calcd. for $C_{42}H_{30}F_6N_8O_6RuS{\cdot}H_2O$: C, 50.05; N, 11.12; H, 3.20. Found: C, 50.28; N, 11.01; H, 3.10.

Selected spectral data of **TF-28**. MS (FAB, ^{102}Ru): m/z 1049 $(M+1)^+$. ^{1}H NMR (400 MHz, d_6-DMSO, 298 K): δ 9.31(s, 2H), 9.12 (s, 2H), 8.49 (s, 1H), 8.39 (s, 1H), 7.68 (d, J_{HH} = 5.6 Hz, 2H), 7.64 (d, J_{HH} = 5.6 Hz, 2H), 7.36 (s, 1H), 7.12 (s, 1H), 4.56 ~ 4.51 (m,

2H), 4.41 ~ 4.35 (m, 2H), 2.76 (t, J_{HH} = 8 Hz, 2H), 1.67 (quin, J_{HH} = 8 Hz, 2H), 1.45 ~ 1.36 (m, 6H), 1.07 (t, J_{HH} = 8 Hz, 3H). ^{19}F NMR (376 MHz, d_6-DMSO, 298 K): δ -58.33 (s, 3F), -68.24 (s, 3F). Anal. Calcd. for $C_{44}H_{32}F_6N_8O_8RuS\cdot 2H_2O$: C, 48.76; N, 10.34; H, 3.35. Found: C, 48.63; N, 10.02; H, 3.04.

Acknowledgments

This work was supported by the National Science Council of Taiwan. The computation was conducted at the National Center for High-Performance Computing (NCHC) and we are grateful to the NCHC for computer time and facilities.

Reference

1. M. K. Nazeeruddin, A. Kay, I. Rodicio, R. Humphry-Baker, E. Mueller, P. Liska, N. Vlachopoulos and M. Grätzel, *J. Am. Chem. Soc.*, 1993, **115**, 6382.
2. M. Grätzel, *Acc. Chem. Res.*, 2009, **42**, 1788.
3. A. Yella, H.-W. Lee, H. N. Tsao, C. Yi, A. K. Chandiran, M. K. Nazeeruddin, E. W.-G. Diau, C.-Y. Yeh, S. M. Zakeeruddin and M. Grätzel, *Science*, 2011, **334**, 629.
4. M. J. Griffith, K. Sunahara, P. Wagner, K. Wagner, G. G. Wallace, D. L. Officer, A. Furube, R. Katoh, S. Mori and A. J. Mozer, *Chem. Commun.*, 2012, **48**, 4145.
5. B. E. Hardin, H. J. Snaith and M. D. McGehee, *Nat. Photonics*, 2012, **6**, 162.
6. M. K. Nazeeruddin, P. Péchy, T. Renouard, S. M. Zakeeruddin, R. Humphry-Baker, P. Comte, P. Liska, L. Cevey, E. Costa, V. Shklover, L. Spiccia, G. B. Deacon, C. A. Bignozzi and M. Grätzel, *J. Am. Chem. Soc.*, 2001, **123**, 1613.
7. Y. Chiba, A. Islam, R. Komiya, N. Koide and L. Han, *Appl. Phys. Lett.*, 2006, **88**, 223505.
8. H. Ozawa, R. Shimizu and H. Arakawa, *RSC Advances*, 2012, **2**, 3198.
9. P. Wang, S. M. Zakeeruddin, J. E. Moser, M. K. Nazeeruddin, T. Sekiguchi and M. Grätzel, *Nat. Mater.*, 2003, **2**, 402.
10. M. K. Nazeeruddin, F. De Angelis, S. Fantacci, A. Selloni, G. Viscardi, P. Liska, S. Ito, B. Takeru and M. Grätzel, *J. Am. Chem. Soc.*, 2005, **127**, 16835.
11. T. Bessho, E. Yoneda, J.-H. Yum, M. Guglielmi, I. Tavernelli, H. Imai, U. Rothlisberger, M. K. Nazeeruddin and M. Grätzel, *J. Am. Chem. Soc.*, 2009, **131**, 5930.
12. P. G. Bomben, T. J. Gordon, E. Schott and C. P. Berlinguette, *Angew. Chem. Int.*

Ed., 2011, **50**, 10682.

13. F. Gajardo, M. Barrera, R. Vargas, I. Crivelli and B. Loeb, *Inorg. Chem.*, 2011, **50**, 5910.
14. K. C. D. Robson, B. D. Koivisto, A. Yella, B. Sporinova, M. K. Nazeeruddin, T. Baumgartner, M. Grätzel and C. P. Berlinguette, *Inorg. Chem.*, 2011, **50**, 5494.
15. Y. Qin and Q. Peng, *Int. J. Photoenergy*, 2012, 291579.
16. S. P. Singh, K. S. V. Gupta, G. D. Sharma, A. Islam and L. Han, *Dalton Trans.*, 2012, **41**, 7604.
17. K. C. D. Robson, P. G. Bomben and C. P. Berlinguette, *Dalton Trans.*, 2012, **41**, 7814.
18. T. Funaki, H. Funakoshi, N. Onozawa-Komatsuzaki, K. Kasuga, K. Sayama and H. Sugihara, *Chem. Lett.*, 2012, **41**, 647.
19. L. E. Polander, A. Yella, B. F. E. Curchod, A. N. Ashari, J. Teuscher, R. Scopelliti, P. Gao, S. Mathew, J.-E. Moser, I. Tavernelli, U. Rothlisberger, M. Gratzel, M. K. Nazeeruddin and J. Frey, *Angew. Chem. Int. Ed.*, 2013, **52**, 8731.
20. T. Funaki, N. Onozawa-Komatsuzaki, K. Kasuga, K. Sayama and H. Sugihara, *Inorg. Chem. Commun.*, 2013, **35**, 281.
21. C. Dragonetti, A. Colombo, M. Magni, P. Mussini, F. Nisic, D. Roberto, R. Ugo, A. Valore, A. Valsecchi, P. Salvatori, M. G. Lobello and F. D. Angelis, *Inorg. Chem.*, 2013, **52**, 10723.
22. G. D. Sharma, S. P. Singh, R. Kurchania and R. J. Ball, *RSC Advances*, 2013, **3**, 6036.
23. P. T. Nguyen, A. R. Andersen, E. M. Skou and T. Lund, *Sol. Energy Mater. Sol. Cells*, 2010, **94**, 1582.
24. S. H. Wadman, J. M. Kroon, K. Bakker, M. Lutz, A. L. Spek, G. P. M. van Klink and G. van Koten, *Chem. Commun.*, 2007, 1907.
25. S. H. Wadman, M. Lutz, D. M. Tooke, A. L. Spek, F. Hartl, R. W. A. Havenith, G. P. M. van Klink and G. van Koten, *Inorg. Chem.*, 2009, **48**, 1887.
26. K. C. D. Robson, B. D. Koivisto and C. P. Berlinguette, *Inorg. Chem.*, 2012, **51**, 1501.
27. B. Schulze, D. G. Brown, K. C. D. Robson, C. Friebe , M. Jäger , E. Birckner, C. P. Berlinguette and U. S. Schubert *Chem. Eur. J.*, 2013, **19**, 14171.
28. M. Chandrasekharam, T. Suresh, S. P. Singh, B. Priyanka, K. Bhanuprakash, A. Islam, L. Han and M. Lakshmi Kantam, *Dalton Trans.*, 2012, **41**, 8770.
29. S.-W. Wang, K.-L. Wu, E. Ghadiri, M. G. Lobello, S.-T. Ho, Y. Chi, J.-E. Moser, F. De Angelis, M. Grätzel and M. K. Nazeeruddin, *Chem. Sci.*, 2013, **4**, 2423.
30. T. Moehl, H. N. Tsao, K.-L. Wu, H.-C. Hsu, Y. Chi, E. Ronca, F. De Angelis, M. K. Nazeeruddin and M. Grätzel, *Chem. Mater.*, 2013, **25**, 4497.

31. K.-L. Wu, H.-C. Hsu, K. Chen, Y. Chi, M.-W. Chung, W.-H. Liu and P.-T. Chou, *Chem. Commun.*, 2010, **46**, 5124.
32. C.-C. Chou, K.-L. Wu, Y. Chi, W.-P. Hu, S. J. Yu, G.-H. Lee, C.-L. Lin and P.-T. Chou, *Angew. Chem. Int. Ed.*, 2011, **50**, 2054.
33. C.-W. Hsu, S.-T. Ho, K.-L. Wu, Y. Chi, S.-H. Liu and P.-T. Chou, *Energy Environ. Sci.*, 2012, **5**, 7549.
34. K.-L. Wu, W.-P. Ku, J. N. Clifford, E. Palomares, S.-T. Ho, Y. Chi, S.-H. Liu, P.-T. Chou, M. K. Nazeeruddin and M. Grätzel, *Energy Environ. Sci.*, 2013, **6**, 859.
35. K.-L. Wu, W.-P. Ku, S.-W. Wang, A. Yella, Y. Chi, S.-H. Liu, P.-T. Chou, M. K. Nazeeruddin and M. Grätzel, *Adv. Funct. Mater.*, 2013, **23**, 2285.
36. M. A. Elban, W. Sun, B. M. Eisenhauer, R. Gao and S. M. Hecht, *Org. Lett.*, 2006, **8**, 3513.
37. X. Zheng, B. Song and B. Xu, *Eur. J. Org. Chem.*, 2010, 4376.
38. S. C. Ceide and A. G. Montalban, *Tetra. Lett.*, 2006, **47**, 4415.
39. A. Miyashita, Y. Suzuki, K. Ohta and T. Higashino, *Heterocycles*, 1994, **39**, 345.
40. J. Easmon, G. Puerstinger, K.-S. Thies, G. Heinisch and J. Hofmann, *J. Med. Chem.*, 2006, **49**, 6343.
41. M.-W. Chung, T.-Y. Lin, C.-C. Hsieh, K.-C. Tang, H. Fu, P.-T. Chou, S.-H. Yang and Y. Chi, *J. Phys. Chem. A*, 2010, **114**, 7886.
42. J. Suh and W. J. Kwon, *Bioorg. Chem.*, 1998, **26**, 103.
43. H. Ait-Haddou, E. Bejan, J.-C. Daran, G. G. A. Balavoine, F. Berruyer-Penaud, L. Bonazzola, H. Smaoui-Chaabouni and E. Amouyal, *J. Chem. Soc. Dalton Trans*, 1999, 3095.
44. K.-S. Chen, W.-H. Liu, Y.-H. Wang, C.-H. Lai, P.-T. Chou, G.-H. Lee, K. Chen, H.-Y. Chen, Y. Chi and F.-C. Tung, *Adv. Funct. Mater.*, 2007, **17**, 2964.
45. A. Hagfeldt, G. Boschloo, L. Sun, L. Kloo and H. Pettersson, *Chem. Rev.*, 2010, **110**, 6595.
46. Y.-S. Yen, Y.-C. Chen, Y.-C. Hsu, H.-H. Chou, J. T. Lin and D.-J. Yin, *Chem. Eur. J.*, 2011, **17**, 6781.
47. J.-F. Yin, M. Velayudham, D. Bhattacharya, H.-C. Lin and K.-L. Lu, *Coord. Chem. Rev.*, 2012, **256**, 3008.
48. Y.-S. Yen, H.-H. Chou, Y.-C. Chen, C.-Y. Hsu and J. T. Lin, *J. Mater. Chem.*, 2012, **22**, 8734.
49. Y. Ooyama and Y. Harima, *ChemPhysChem*, 2012, **13**, 4032.
50. S.-R. Li, C.-P. Lee, H.-T. Kuo, K.-C. Ho and S.-S. Sun, *Chem. Eur. J.*, 2012, **18**, 12085.
51. B.-G. Kim, K. Chung and J. Kim, *Chem. Eur. J.*, 2013, **19**, 5220.
52. Y. Wu and W. Zhu, *Chem. Soc. Rev.*, 2013, **42**, 2039.

53. F. Gao, Y. Wang, D. Shi, J. Zhang, M. Wang, X. Jing, R. Humphry-Baker, P. Wang, S. M. Zakeeruddin and M. Grätzel, *J. Am. Chem. Soc.*, 2008, **130**, 10720.
54. W.-H. Liu, I.-C. Wu, C.-H. Lai, C.-H. Lai, P.-T. Chou, Y.-T. Li, C.-L. Chen, Y.-Y. Hsu and Y. Chi, *Chem. Commun.*, 2008, 5152.
55. K. Lim, C. Kim, J. Song, T. Yu, W. Lim, K. Song, P. Wang, N. Zu and J. Ko, *J. Phys. Chem. C*, 2011, **115**, 22640.
56. W. Zeng, Y. Cao, Y. Bai, Y. Wang, Y. Shi, M. Zhang, F. Wang, C. Pan and P. Wang, *Chem. Mater.*, 2010, **22**, 1915.
57. A. Listorti, B. O'Regan and J. R. Durrant, *Chem. Mater.*, 2011, **23**, 3381.
58. X. Yang, M. Yanagida and L. Han, *Energy Environ. Sci.*, 2013, **6**, 54.
59. T. Funaki, H. Funakoshi, O. Kitao, N. Onozawa-Komatsuzaki, K. Kasuga, K. Sayama and H. Sugihara, *Angew. Chem. Int. Ed.*, 2012, **51**, 7528.
60. F.-C. Hu, S.-W. Wang, M. Planells, N. Robertson, H. Padhy, B.-S. Du, Y. Chi, P.-F. Yang, H.-W. Lin, G.-H. Lee and P.-T. Chou, *ChemSusChem*, 2013, **6**, 1366.
61. H.-H. Yeh, S.-T. Ho, Y. Chi, J. N. Clifford, E. Palomares, S.-H. Liu and P.-T. Chou, *J. Mater. Chem. A*, 2013, **1**, 7681.
62. K.-L. Wu, S.-T. Ho, C.-C. Chou, Y.-C. Chang, H.-A. Pan, Y. Chi and P.-T. Chou, *Angew. Chem. Int. Ed.*, 2012, **51**, 5642.
63. C.-C. Chou, F.-C. Hu, H.-H. Yeh, H.-P. Wu, Y. Chi, J. N. Clifford, E. Palomares, S.-H. Liu, P.-T. Chou and G.-H. Lee, *Angew. Chem. Int. Ed.*, 2013, DOI: 10.1002/anie.201305975.
64. A. C. Onicha and F. N. Castellano, *J. Phys. Chem. C*, 2010, **114**, 6831.
65. Q. Yu, Y. Wang, Z. Yi, N. Zu, J. Zhang, M. Zhang and P. Wang, *ACS Nano*, 2010, **4**, 6032.
66. P. G. Johansson, J. G. Rowley, A. Taheri, G. J. Meyer, S. P. Singh, A. Islam and L. Han, *Langmiur*, 2011, **27**, 14522.
67. Y. Shi, Y. Wang, M. Zhang and X. Dong, *Phys. Chem. Chem. Phys.*, 2011, **13**, 14590.
68. K. C. D. Robson, K. Hu, G. J. Meyer and C. P. Berlinguette, *J. Am Chem. Soc.*, 2013, **135**, 1961.
69. D. Credgington and J. R. Durrant, *J. Phys. Chem. Lett.*, 2012, **3**, 1465.
70. P. R. F. Barnes, K. Miettunen, X. Li, A. Y. Anderson, T. Bessho, M. Grätzel and B. C. O'Regan, *Adv. Mater.*, 2013, **25**, 1881.
71. S. M. Zakeeruddin and M. Grätzel, *Adv. Funct. Mater.*, 2009, **19**, 2187.
72. J. Halme, P. Vahermaa, K. Miettunen and P. Lund, *Adv. Mater.*, 2010, **22**, E210.
73. F. Fabregat-Santiago, J. Bisquert, G. Garcia-Belmonte, G. Boschloo and A. Hagfeldt, *Sol. Energy Mater. Sol. Cells*, 2005, **87**, 117.
74. F. Sauvage, S. Chhor, A. Marchioro, J.-E. Moser and M. Grätzel, *J. Am. Chem.*

Soc., 2011, **133**, 13103.

TOC Illustration:

Systematic changing the ancillary chelate from **L3** to **L6**, together with addition of 3,4-ethylenedioxythiophene (EDOT) appendage, boosts the overall efficiencies of fabricated DSC device.